Article

# Atomistic Origin of Phase Stability in Oxygen-Functionalized MXene: A Comparative Study

Avanish Mishra,[†][iD] Pooja Srivastava,[†,⊥] Abel Carreras,[‡] Isao Tanaka,[‡,§] Hiroshi Mizuseki,[∥] Kwang-Ryeol Lee,[∥] and Abhishek K. Singh[*,†][iD]

[†]Materials Research Centre, Indian Institute of Science, Bangalore 560012, India

[‡]Department of Materials Science and Engineering and [§]Center for Elements Strategy Initiative for Structural Materials, Kyoto University, Kyoto 606-8501, Japan

[∥]Computational Science Research Center, Korea Institute of Science and Technology (KIST), Seoul 02792, Republic of Korea

[⊥]Amity University, Lucknow Campus, Noida, Uttar Pradesh, India

**S** *Supporting Information*

**ABSTRACT:** Oxygen-functionalized MXene, $M_2CO_2$ (M = group III−V metals), are emergent formidable two-dimensional (2D) materials with a tantalizing possibility for device applications. Using first-principles calculations, we perform an intensive study on the stability of fully O-functionalized ($M_2CO_2$) MXenes. Depending on the position of O atoms, the $M_2CO_2$ can exist in two different structural phases. On one side of MXene, the O atom occupies a site which is exactly on the top of the metal atom from the opposite side. On the other side, the O atom can occupy either the site on the top of the metal atom of the opposite side (BB′ phase) or on the top of the C atom (CB phase). We find that for M = Sc and Y the CB phase is stable, whereas for M = Ti, Zr, Hf, V, Nb, and Ta the stable phase is BB′. The electron localization function, the atom-projected density of states, the charge transfer, and the Bader charge analyses provide a rational explanation for the relative stability of these two phases and justify the ground state structure by giving information about the preferential site of adsorption for the O atoms. We also calculate the phonon dispersion relations for both phases of $M_2CO_2$. The BB′-$Sc_2CO_2$ and the CB-$Ti_2CO_2$ are found to be dynamically unstable. Finally, we find that the instability of BB′-$M_2CO_2$ (M = Sc and Y) originates from the weakening of M−C interactions, which manifest as a phonon mode with imaginary frequency corresponding to the motion of C atom in the $a-b$ plane. The insight into the stability of these competing structural phases of $M_2CO_2$ presented in this study is an important step in the direction of identifying the stable phases of these 2D materials.
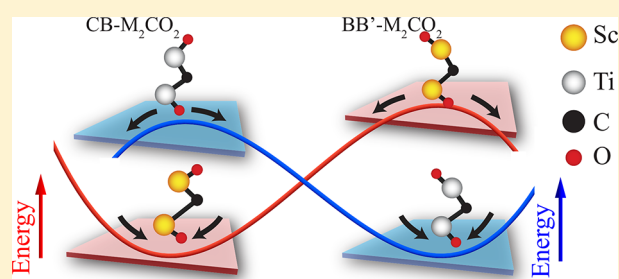
## ■ INTRODUCTION

Recently, a new family of two-dimensional materials (2D), called MXene with chemical formula $M_{n+1}C_n$ (M = early transition metal, C = carbon, $n$ = 1−3),[1,2] have gained a significant interest due to its technological importance. The unusual combination of metallic and ceramic properties, such as good electrical and thermal conductivity as well as high chemical and thermal stability,[2] brings an excellent opportunity for the development of MXene-based energy storage systems,[3−6] catalyst[7−9] support for nanoparticles,[8] and size lead-storage[10] and charge selective ion-sieve[11] devices.

MXenes are generally synthesized by extracting the "A" (groups IIIA−VA) element from the corresponding MAX phase[1] using aqueous hydrofluoric acid. This leaves reactive metal atoms exposed, which almost immediately gets functionalized during exfoliation process.[1,2,12,13] Similar to other 2D materials, the properties of MXene are sensitive to the type of functional group present on the surface. This makes functionalization a powerful tool to engineer the mechanical, electronic, optical, transport, and magnetic properties. For

example, the nonmagnetic $V_2C$ becomes an antiferromagnet, when F/OH functional group is adsorbed on MXene surface.[14] Transport calculations using the nonequilibrium Green's function (NEGF) method have predicted 4 times larger current at a given bias in $Ti_3C_2F_2$ than that of pristine MXene ($Ti_3C_2$).[15]

Recently, a theoretical study[16] predicted the presence of a semiconducting gap in most of the fully O-functionalized MXenes. These semiconducting O-functionalized MXene are proposed as promising for electronics,[17−21] thermoelectric,[16,22] hydrogen storage,[23,24] gas sensing,[25] lead storage,[10] photocatalysis,[26] and optoelectronic[27] applications. Surface termination by O atoms essentially plays a crucial role in opening the gap in otherwise metallic $M_2C$ MXenes (Figure 1a).[1,2,13,28] It has been shown[16] that the crystal symmetry of O-functionalized MXene and therefore their semiconducting band gaps critically
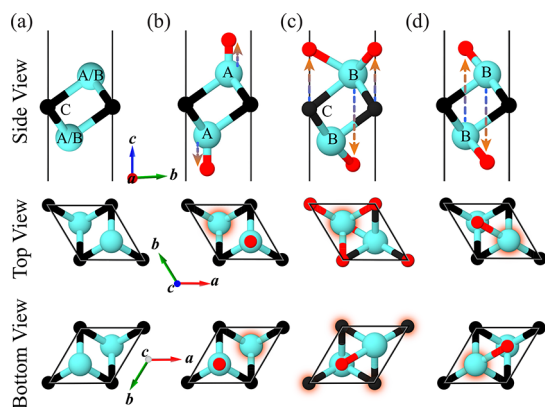
**Figure 1.** Structures of the different possible phases of O-functionalized MXenes together with the structure of pristine MXene. (a) Structure of pristine MXene with possible O adsorption sites, which are labeled as A, B, and C. This structure does not include any O atom. (b, c, d) Structures of O-functionalized AA, CB, and BB′ phases, respectively. The red glow indicates the position of the oxygen atoms on the opposite side, which are not visible.

depend upon the transition metal M. The unit cell of a MXene contains two metal atoms connected by a carbon atom. These two metal atoms are not aligned in the vertical direction. During functionalization, the first oxygen atoms gets adsorbed at a site, which is exactly on top of the metal atom on the opposite side (B). Once the first O atom is adsorbed at B site, there are two preferred sites for the adsorption of the next O atom on the opposite side of the MXene. One of them is located right above the metal atom from the opposite side (B′), whereas the other one is on top of the carbon atom (C). On the basis of the adsorption site for the second O atom, we refer the two possible phases as BB′ and CB,[29,30] which are shown in Figure 1.

Khazai et al.[16] studied the ground state structures of several MXenes. To explain the preference for a particular crystal structure, the maximum possible oxidation state of M is considered as an important parameter.[16] As the M−C bonding character is not purely ionic or covalent, the formation of these phases cannot be understood completely by merely considering the oxidation states of M atoms. Atom-projected density of states (DOS) calculations indicate strong hybridization between d-states of M and p-states of O and C atoms.[16] Recently, based on the comparison of total energy and phonon calculations, the stable ground state structures were identified for several $M_2CT_2$ (M = groups III−VI, T = F/OH) MXenes.[7] However, the origin of the stability of these phases of $M_2CO_2$ remains an open question.

Using density-functional theory (DFT), herein we unravel the origin of the stability of the two competing phases: CB and BB′ of $M_2CO_2$ (M = groups III−V). Negative formation energies are obtained for all the O-functionalized MXenes considered here, indicating that the oxidation of MXenes is energetically favorable. Simple structural analysis shows the presence of strong M−C and M−O bonds in both phases of $M_2CO_2$ (M = groups IV−V). However, weakly bonded C atoms were identified in BB′ phase of $M_2CO_2$ (M = group III). The study of the electron localization function (ELF) and the atom-projected density of states of pristine, $M_2CO$, and $M_2CO_2$ provides a rational explanation for the preferred site of adsorption of O atoms and the formation of the ground state structure of $M_2CO_2$. Charge transfer and Bader charge analyses

show the relative strength of similar bonds in both phases. Phonon calculations are also performed to assess the dynamical stability of these phases of O-functionalized MXenes. We find real positive frequency throughout the Brillouin zone for CB and BB′, the lowest energy phases of O-functionalized $Sc_2C$ and $Ti_2C$ MXenes, respectively. In line with the ELF and DOS analysis, we identify imaginary phonon frequencies as a consequence of the motion of the C atoms in the a−b plane of BB′-$M_2CO_2$ (M = Sc and Y). The present study provides an in-depth understanding of the stability of the ground state structure of these O-functionalized MXenes, which we expect will increase the interest in experimental analysis of these semiconducting MXenes.

## METHODOLOGY

The calculations were performed within the framework of density functional theory (DFT) using the Vienna *ab initio* Simulation Package (VASP).[31] The wave functions are expressed in a plane wave basis set with an energy cutoff of 500 eV. The potentials at the core region are treated with projector augmented wave (PAW) pseudopotentials.[32] The exchange-correlation energy is represented by a gradient corrected[32,33] functional proposed by Perdew, Burke, and Ernzerhof (PBE).[34] Brillouin zone integrations were performed using a 13 × 13 × 1 Monkhorst−Pack[35] k-point mesh. The geometrical parameters of unit cell were optimized using the conjugate gradient scheme until each component of the forces on every atom were ≤0.001 eV/Å. The convergence of geometrical parameters was also tested. For density of states calculations the Brillouin zone was sampled using a 15 × 15 × 1 k-grid. In all the structures, vacuum regions between two adjacent periodic images were fixed to 20 Å to avoid spurious interaction between periodic images. Phonon frequencies were calculated using the PHONOPY package,[36] which uses the force constants calculated using the finite difference technique. Forces were calculated using the 4 × 4 × 1 supercell of the conventional cell.

## RESULTS AND DISCUSSION

Functionalization is an attractive route for controlling the electronic properties of 2D materials. By modifying the topology of these sheets locally, the functional group affects the electronic properties of the materials considerably. As described before, the pristine MXene has three possible adsorption sites, which are labeled as A, B, and C as shown in Figure 1a. In agreement with earlier studies, in our calculations we find that A site (Figure 1b) is the least favorable[16] for the O adsorption.

To understand the feasibility of O functionalization, we calculate the formation energy ($E^f$) of $M_2CO_2$ taking the pristine MXene and $O_2$ molecule as the reference state for MXene and O atom, respectively. We define $E^f$ as

$$E^f = E_{M_2CO_m} - E_{M_2C} - m\frac{1}{2}\mu_{O_2} \qquad (1)$$

where $E_{M_2C}$ and $E_{M_2CO_m}$ are the energies of the pristine and O-functionalized MXene, respectively. $\mu_{O_2}$ is the chemical potential of the $O_2$ molecule. Here m defines the number of O atoms in the O-functionalized MXenes. Our calculations show that for both the phases of O-functionalized MXene the formation energies are negative, as shown in Figure 2. This indicates that the functionalization of MXene with O is
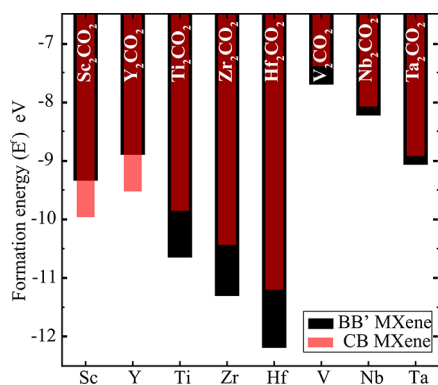
**Figure 2.** Formation energies of CB and BB′ phases of O-functionalized MXene, $M_2CO_2$, where M belongs to groups III−V.

energetically favorable. However, the relative stability of both phases of O-functionalized MXenes crucially depends upon M atom.[7,16,37] If M belongs to group III, the CB phase is preferred; otherwise, the BB′ phase is more favorable. As shown in Figure 2, for M = group III, the $E^f$ increases with increasing period within the same group for both phases. For M = groups IV−V, the energy decreases with increasing period. Based on their ground state structures, O-functionalized MXenes ($M_2CO_2$, M = groups III−V) can be divided into two categories: one forming BB′ phase (groups IV−V) and the other forming CB phase (group III). $Sc_2CO_2$ (III) and $Ti_2CO_2$ (IV) are taken as representatives of the O-functionalized MXenes in these two categories. The results of these two O-functionalized MXenes are presented here.

The symmetries of the CB and the BB′ phases are $P3m1$ and $P\bar{3}m1$, respectively. The BB′ has an inversion symmetry about $a/b$ and $c$ planes. Because of this inversion symmetry, both the C−M bonds are of equal length. However, in the CB phase, two different kinds of C−M bonds can be observed due to the absence of inversion symmetry (Figure 3). Bond lengths of the
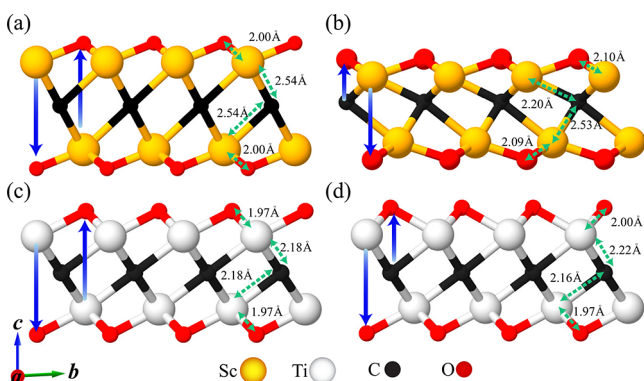


**Figure 3.** Side view of (a) BB′ and (b) CB phases of $Sc_2CO_2$ and (c) BB′ and (d) CB phases of $Ti_2CO_2$. Bond lengths are also shown here. The positions of O atoms are highlighted by blue arrows.

CB and BB′ phases of $Sc_2CO_2$ and $Ti_2CO_2$ are shown in Figure 3. The lengths of both Sc−O bonds (Table S1) are shorter than the sum of the covalent radii of Sc and O, indicating the presence of strong Sc−O bonds. Both the Sc−C bonds in BB′ phase and one Sc−C bond (~2.53 Å) in CB phase are larger than the sum of the covalent radii of Sc and C, indicating that these bonds are relatively weak. In the CB phase of $Sc_2CO_2$, the length of one Sc−C bond (2.20 Å) is close to the sum of the

covalent radii of Sc and C (2.21 Å). We observed a similar trend in $Y_2CO_2$ (Table S1).

On the other hand, in both CB and BB′ phases of $Ti_2CO_2$, the lengths of all Ti−C bonds are longer than the sum of the covalent radii of Ti and C (2.13 Å). In BB′ phase both Ti−C bonds are slightly longer (0.05 Å) than the sum of the covalent radii of Ti and C. In CB phase, one of the Ti−C bond is 0.03 Å and other is 0.09 Å longer than the sum of the covalent radii of Ti and C. The relatively large difference of the Ti−C bond from the sum of the covalent radii is in agreement with the difference in $E^f$ of the two phases. As presented in Table S1, the relative bond lengths of other $M_2CO_2$, M = group IV, have similar values and therefore are expected to follow similar behavior.

In order to understand the relative stabilities of these two phases, we performed an electron localization function (ELF) analysis, which measures the localization of pairs of electrons. The value of ELF between two atoms can be in the range of 0 to 1, where 1, 0.5, and 0 represent covalent, metallic, and no-bonding character, respectively. Figure 4 shows the ELF for
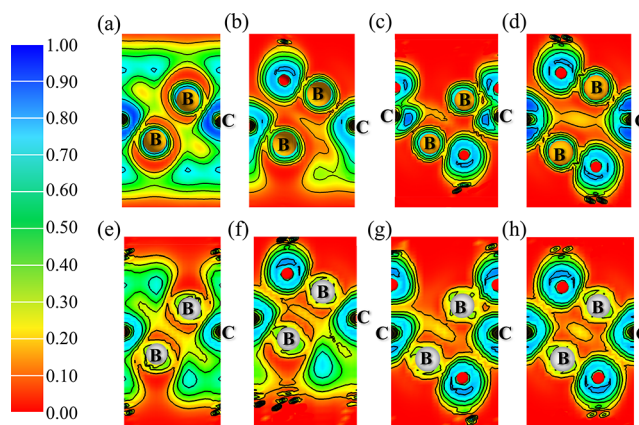


**Figure 4.** 2D slices projected along [110] direction of electron localization function (ELF) are plotted. Upper panel shows the ELF plots for (a) $Sc_2C$, (b) $Sc_2CO$, (c) CB-$Sc_2CO_2$, (d) BB′-$Sc_2CO_2$, and lower panel shows the ELF for (e) $Ti_2C$, (f) $Ti_2CO$, (g) CB-$Ti_2CO_2$, and (h) BB′-$Ti_2CO_2$. Orange, white, black, and red balls represent Sc, Ti, C, and O atoms, respectively.

$M_2C$ (M = Sc, Ti) and $M_2CO$ and $M_2CO_2$ on the (110) plane, which passes through the metal and oxygen atoms. In pristine MXene (Figure 4a,e), we observe ELF ~ 0.15−0.8 between M and C together with a strong localization of electrons (ELF ~ 0.8) near C atoms that show the metallic−ionic character of the M−C bonds. In pristine $Sc_2C$ MXene, we observe a region of localized ELF ~ 0.7 over both B and C sites (Figure 4a). As M is more electropositive compared to carbon, oxygen prefers to adsorb over the B site (Figure 4a,b). On the other hand, in $Ti_2C$, ELF ~ 0.7 is localized over the B site (Figure 4e) and the first O gets adsorbed there. Interestingly, after the adsorption of the first O atom on one side, a highly localized ELF ~ 0.5−0.7 appears over C and B′ site in $Sc_2CO$ and $Ti_2CO$, respectively, as shown in Figure 4b,f. This shows the electronic origin of the preferred formation of CB and BB′ phases over the other phases in $Sc_2CO_2$ and $Ti_2CO_2$, respectively. Although ELF ~ 0.2−0.8 is observed between Sc−C and Sc−O atoms (Figure 4c and Figure S3a) in both CB and BB′ phases, the strong localization of ELF ~ 0.5−0.75 between C and O atoms further stabilizes the CB phase of $Sc_2CO_2$. In contrast, the presence of
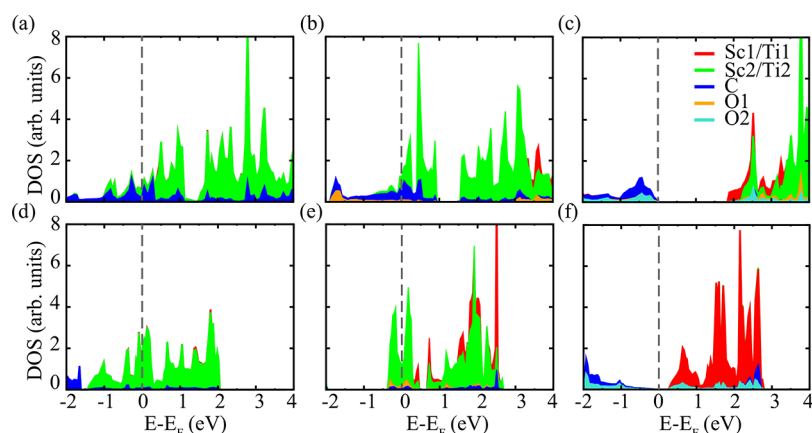
**Figure 5.** Upper panels show the atom projected density of states of (a) $Sc_2C$, (b) $Sc_2CO$, and (c) $CB-Sc_2CO_2$. Lower panels show the atom projected density of states of (d) $Ti_2C$, (e) $Ti_2CO$, and (f) $BB'-Ti_2CO_2$. To distinguish the two M and two O atoms, we label them as 1 and 2 for first and second layer as shown in Figure S1.

weakly localized ELF $\sim 0$ between O and C atoms (Figure 4d and Figure S3b) in $BB'-Sc_2CO_2$ indicates the instability of this phase. As shown in Figure 4c, the ionic character of Sc—C and Sc—O can be concluded from the large value of ELF $\sim 0.8$ near the C and O atoms in $CB-Sc_2CO_2$. In the CB phase of $Ti_2CO_2$, the ELF is $\sim 0$ between one Ti and O atoms, which makes it a less favorable structure (Figure 4f and Figure S3c). In $Ti_2CO_2$, the weakly localized electron density is visible along all the Ti—C, Ti—O, and C—O bonds in the $BB'$ phase (Figure 4h and Figure S3d).

The ELF provides a rational explanation for the preference for $BB'/CB$ phases in these MXenes. To understand the bonding strengths, we next perform a Bader charge analysis. Charge transfer plays an important role in the strength of bonds. The larger the charge transfer between the atoms, the stronger is the bond. A quantitative estimation of charge transfer using the Bader charge analysis is presented in Figure S4. Following the electronegativity difference (O > C > Ti > Sc), the charge is always transferred to C and O atoms from the metals. O atoms draw charges from other atoms in $M_2CO_2$. For $Sc_2CO_2$, less charge is gained by the top O atoms in the CB phase compared to the $BB'$ phase. Therefore, the bonding between Sc and O atoms is stronger in $BB'$ phase as shown in Figure S3a,b. Large charge transfer from Sc to O atoms results in less charge transfer between Sc and C atom, and therefore the bonding between those becomes weaker. In $CB-Sc_2CO_2$, the overall charge gained by C atom is small due to direct transfer of charge from C to O atom, leading to stronger bonding between C and O atoms relative to the $BB'$ phase. Similar arguments can be used to explain the stronger bonding between Ti—C and Ti—O atoms in $BB'$ phase of $Ti_2CO_2$ (Figure S3c,d). Stronger bonding implies higher stability of the phase; hence, $CB-Sc_2CO_2$ and $BB'-Ti_2CO_2$ are more stable than the other phases. A more detailed description of charge transfer is also shown using the charge accumulation and depletion analysis shown in Figure S5.

To further illustrate the preference for a given phase, we analyzed the electronic structure of the $BB'$ and the CB phases of $M_2CO_2$ (M = Sc, Ti). We calculated the atom-projected density of states of pristine, $M_2CO$, CB, and $BB'-M_2CO_2$ (Figure 5). The presence of 3d states of the Sc atom around the Fermi level renders the pristine $M_2C$ MXene metallic (Figure 5a). Strong hybridization between Sc 3d and C 2p states below the Fermi level can be observed in Figure 5a,

which indicates a strong bonding between these atoms. The presence of Sc 3d states at the Fermi level in pristine MXene makes the Sc atom more reactive than the C atom. At A site, O states can hybridize with the states of only one metal atom; however, on the B site, O states can effectively hybridize with the 3d states of nearby three metal atoms. Therefore, for the adsorption of first O atom the metal top site B is preferred. As shown above, due to the large electronegativity difference between the Sc and O atoms, the electrons are transferred from Sc to O. Therefore, the empty Sc states appear above the Fermi level (Figure 5b), and filled O states appear below the Fermi level. C atom mainly contributes to the states around the Fermi level, indicating the high chemical reactivity of the C atom. Therefore, the C-top site is more preferable for the adsorption of second O atom (Figure 5c) than the B site, leading to formation of the CB phase for $Sc_2CO_2$. The strong bonding of Sc with O and C can be inferred from the overlap between Sc states and O/C states in the CB phase. The strong hybridization of states of C and O pushes the C states to lower energy, leading to the opening of a semiconducting gap in the CB phase. In the $BB'$ phase, the interaction between Sc and O on both sides of MXene weakens the Sc—C bond, as can be observed from the weak overlap between the Sc and C states. Furthermore, the C states appear at the Fermi level making the $BB'-Sc_2CO_2$ metallic (Figure S6a). Weak Sc—C bonds and the presence of high density C p-states at the Fermi level destabilizes the metallic $BB'$ phase, whereas strong Sc—C/O bonds and large semiconducting gap makes the CB phase stable.

Similar to pristine $Sc_2C$, in the case of $Ti_2C$, the C atom draws charge from Ti atom and, due to one extra electron in Ti 3d states, the bonding states of C atom go lower in energy. The presence of partially filled Ti 3d states at the Fermi level makes the metal atoms chemically more active than the C atoms and results in the adsorption of first O atom on the B site (Figure 5e). As soon as the O atom gets adsorbed over the B site, it draws electrons from Ti, affecting the bonding of Ti with C atoms. This effect can be seen as a upward shift of C states, as shown in Figure 5e. There is a charge transfer from Ti atoms to C (Figure 5e), which brings the states of Ti atoms at the Fermi level, and therefore the B site becomes the most preferred site for the adsorption of the O atom on the opposite side. Hence, the $BB'$ phase is preferred over the CB phase (Figure 5f) for $Ti_2CO_2$. Furthermore, the strong hybridization between 2p

states of O and C atoms and 3d states of the metal atom can be inferred from Figure 5f and Figure S6b. As can be seen, the hybridization and therefore the bonding between Ti 3d states and 2p states of C and O are stronger in the BB′ phase compared to that in the CB phase. The strong bonding between Ti and C/O makes the BB′ phase more stable than the CB phase. After the adsorption of both O atoms, the completely filled C and O bonding states appear below the Fermi level and empty states of Ti appear above the Fermi level. This opens a gap between the valence and conduction bands in both BB′ (Figure 5f) and CB (Figure S6b) phases of $Ti_2CO_2$.

Although ELF and DOS analyses show preference for the formation of CB/BB′ phases for $Sc_2CO_2$/$Ti_2CO_2$, to confirm the dynamical stabilities of these phases, we calculated the phonon band structure. The calculated converged phonon dispersion relations of $M_2CO_2$ (M = Sc and Ti) along the high symmetry directions of the Brillouin zone (BZ) for both CB and BB′ phases are shown in Figure 6. The CB phase of
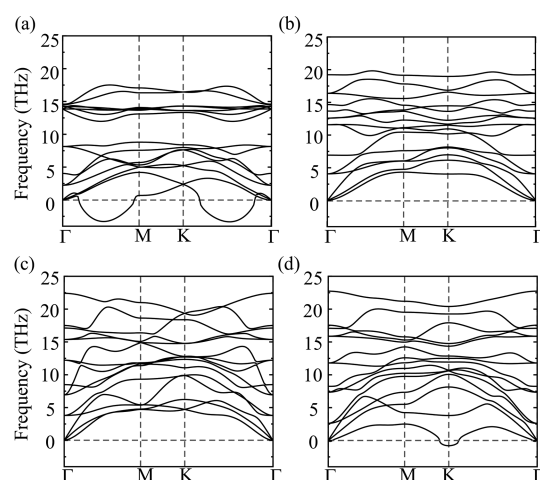


**Figure 6.** Phonon dispersion relations of (a) BB′-$Sc_2CO_2$, (b) CB-$Sc_2CO_2$, (c) BB′-$Ti_2CO_2$, and (d) CB-$Ti_2CO_2$.

$Sc_2CO_2$ (Figure 6b) shows positive real phonon frequencies throughout the BZ; therefore, we conclude that the structure is dynamically stable. However, large imaginary phonon frequencies in the phonon band structure of BB′ phase (Figures 6a and 7a) of $Sc_2CO_2$ reveals that this phase may be dynamically unstable. We have checked the phonon dispersion relations for different supercell sizes varying from 2 × 2 × 1 to 6 × 6 × 1.
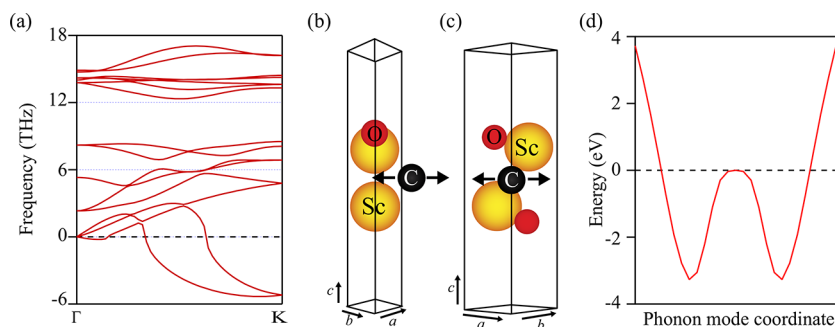
The main features, particularly imaginary frequencies, remained the same as shown in Figure S7. The two degenerate phonon modes associated with these imaginary frequencies mainly correspond to the motion of the C atom along the *a* and *b* directions (Figure 7b,c). This suggests that the C atom may be able to move almost freely along the *a*−*b* plane, which results in the instability of the BB′ phase of $Sc_2CO_2$. In contrast to BB′, in the CB phase due to different bond lengths of two Sc−C bonds the degeneracy is lifted. As one Sc−C bond is shorter than the other bond, the increased interaction between the Sc and C gives rise to positive frequencies at the K-point in the CB phase. This is in agreement with the ELF (Figure 4d) and atom-projected density of states (Figure S6a) of BB′-$Sc_2CO_2$ as discussed above. Finally, we also calculated the profile of the potential energy as a function of phonon displacement corresponding to the imaginary mode in the BB′ phase of $Sc_2CO_2$. As expected, we found a double-well potential around the equilibrium position of the C atom (Figure 7d), which confirms the instability of this phonon modes.

For the BB′ phase of $Ti_2CO_2$, the phonon band structure shows only positive real frequencies throughout the BZ shown in Figure 6c. The high-energy CB phase of $Ti_2CO_2$ shows a softening of one acoustical branch at the K-point as shown in Figure 6d, indicating the instability of this phase. Relative to the BB′ phase of $Sc_2CO_2$, stiffer modes in the BB′ phase of $Ti_2CO_2$ may be due to the presence of one more electron in Ti, which causes a stronger bonding between C and Ti that limits the movement of C atoms.

Even though the negative formation energies indicate the possibility of existence of these phases, a vibrational analysis is essential to determine their stability. This aspect becomes more important for 2D materials, where the number of degrees of freedom are large, which can lead to numerous possible structures. In general, the understanding of the atomistic details, e.g., interaction strengths, spatial electron localizations, etc., as presented in this work, allows to rationally choose the functional groups that can lead to synthesis of stable phases.

## ■ CONCLUSION

Using first-principles calculations, we have studied the relative stabilities of two structural phases of O-functionalized MXenes $M_2CO_2$ (M = groups III−V): CB and BB′. The negative formation energies of both CB and BB′ phases for all the $M_2C$ MXenes indicate a high chance of their synthesis. By analyzing the ELF and the atom-projected DOS of pristine $M_2C$, CB, and BB′ phases of $M_2CO_2$, we have provided a rational justification



**Figure 7.** (a) Phonon band structure of BB′-$Sc_2CO_2$ calculated using the 3 × 3 × 1 supercell of the conventional cell. There are two degenerate imaginary phonon modes at K-points. (b, c) The direction of the C atoms in these modes. (d) Potential energy as a function of the phonon displacement along each of these modes.

for the preferred adsorption site of the O atoms on both sides of MXene. These analyses indicate that CB and BB′ phases are energetically more favorable, if M belongs to groups III and IV−V, respectively. Our calculations of ELF, DOS, charge transfer, and Bader charge analyses reveal the presence of weak Sc−C bonds in the BB′ phase of $Sc_2CO_2$. The dynamical stability of both phases of $M_2CO_2$ has been investigated by phonon calculations. The BB′-$Sc_2CO_2$ and CB-$Ti_2CO_2$ O-functionalized MXenes show imaginary phonon modes, suggesting the dynamical instability of these MXenes. Finally, we proposed that the instability of BB′ phase of $Sc_2CO_2$ may be caused by the motion of the weakly bonded C atom, which agrees well with the electronic structure, ELF, and charge transfer analysis. The atomistic insight developed in this study into the stability of the competing phases of $M_2CO_2$ (M = groups III−V) may be used as a guideline for experimentalists to judiciously choose a functional group that does not compromise the stability of the MXene structure.

## ASSOCIATED CONTENT

### Supporting Information

The Supporting Information is available free of charge on the ACS Publications website at DOI: 10.1021/acs.jpcc.7b06162.

Labels used to refer the atoms of BB′ and CB phases, enlarged ELF plots for $M_2CO$ (M = Sc, Ti), quantitative description of ELF of $M_2CO_2$ (M = Sc, Ti), Bader charge analysis for BB′ and CB phases of $M_2CO_2$ (M = Sc, Ti), charge transfer in BB′ and CB phases of $M_2CO_2$ (M = Sc, Ti), and atom-projected DOS for BB′-$Sc_2CO_2$ and CB-$Ti_2CO_2$, phonon dispersion of CB-$Ti_2CO_2$ MXene for various supercell sizes (Figures S1−S7); geometrical parameters of O-functionalized MXenes and covalent radii of all atoms forming MXenes (Table S1) (PDF)

## AUTHOR INFORMATION

**Corresponding Author**

*E-mail: abhishek@mrc.iisc.ernet.in (A.K.S.).

**ORCID**

Avanish Mishra: 0000-0003-3997-0445
Abhishek K. Singh: 0000-0002-7631-6744

**Notes**

The authors declare no competing financial interest.

## REFERENCES

(1) Naguib, M.; Kurtoglu, M.; Presser, V.; Lu, J.; Niu, J.; Heon, M.; Hultman, L.; Gogotsi, Y.; Barsoum, M. W. Two-Dimensional Nanocrystals Produced by Exfoliation of $Ti_3AlC_2$. *Adv. Mater.* **2011**, 23, 4248−4253.

(2) Naguib, M.; Mochalin, V. N.; Barsoum, M. W.; Gogotsi, Y. 25th Anniversary Article: MXenes: A New Family of Two-Dimensional Materials. *Adv. Mater.* **2014**, 26, 992−1005.

(3) Tang, Q.; Zhou, Z.; Shen, P. Are MXenes Promising Anode Materials for Li Ion Batteries? Computational Studies on Electronic Properties and Li Storage Capability of $Ti_3C_2$ and $Ti_3C_2X_2$ (X = F, OH) Monolayer. *J. Am. Chem. Soc.* **2012**, 134, 16909−16916.

(4) Er, D.; Li, J.; Naguib, M.; Gogotsi, Y.; Shenoy, V. B. $Ti_3C_2$ MXene as a High Capacity Electrode Material for Metal (Li, Na, K, Ca) Ion Batteries. *ACS Appl. Mater. Interfaces* **2014**, 6, 11173−11179.

(5) Xie, Y.; Dall'Agnese, Y.; Naguib, M.; Gogotsi, Y.; Barsoum, M. W.; Zhuang, H. L.; Kent, P. R. C. Prediction and Characterization of MXene Nanosheet Anodes for Non-Lithium-Ion Batteries. *ACS Nano* **2014**, 8, 9606−9615.

(6) Sun, D.; Hu, Q.; Chen, J.; Zhang, X.; Wang, L.; Wu, Q.; Zhou, A. Structural Transformation of MXene ($V_2C$, $Cr_2C$, and $Ta_2C$) with O Groups during Lithiation: A First-Principles Investigation. *ACS Appl. Mater. Interfaces* **2016**, 8, 74−81.

(7) Guo, Z.; Zhou, J.; Zhu, L.; Sun, Z. MXene: A Promising Photocatalyst for Water Splitting. *J. Mater. Chem. A* **2016**, 4, 11446−11452.

(8) Ran, J.; Gao, G.; Li, F.-T.; Ma, T.-Y.; Du, A.; Qiao, S.-Z. $Ti_3C_2$ MXene Co-Catalyst on Metal Sulfide Photo-Absorbers for Enhanced Visible-Light Photocatalytic Hydrogen Production. *Nat. Commun.* **2017**, 8, 13907.

(9) Zhang, X.; Lei, J.; Wu, D.; Zhao, X.; Jing, Y.; Zhou, Z. A Ti-Anchored $Ti_2CO_2$ Monolayer (MXene) as A Single-Atom Catalyst for CO oxidation. *J. Mater. Chem. A* **2016**, 4, 4871−4876.

(10) Peng, Q.; Guo, J.; Zhang, Q.; Xiang, J.; Liu, B.; Zhou, A.; Liu, R.; Tian, Y. Unique Lead Adsorption Behavior of Activated Hydroxyl Group in Two-Dimensional Titanium Carbide. *J. Am. Chem. Soc.* **2014**, 136, 4113−4116.

(11) Ren, C. E.; Hatzell, K. B.; Alhabeb, M.; Ling, Z.; Mahmoud, K. A.; Gogotsi, Y. Charge- and Size-Selective Ion Sieving Through $Ti_3C_2T_x$ MXene Membranes. *J. Phys. Chem. Lett.* **2015**, 6, 4026−4031.

(12) Mishra, A.; Srivastava, P.; Mizuseki, H.; Lee, K.-R.; Singh, A. K. Isolation of Pristine MXene from $Nb_4AlC_3$ MAX Phase: A First-Principles Study. *Phys. Chem. Chem. Phys.* **2016**, 18, 11073−11080.

(13) Srivastava, P.; Mishra, A.; Mizuseki, H.; Lee, K.-R.; Singh, A. K. Mechanistic Insight into the Chemical Exfoliation and Functionalization of $Ti_3C_2$ MXene. *ACS Appl. Mater. Interfaces* **2016**, 8, 24256−24264.

(14) Hu, J.; Xu, B.; Ouyang, C.; Yang, S. A.; Yao, Y. Investigations on $V_2C$ and $V_2CX_2$ (X = F, OH) Monolayer as a Promising Anode Material for Li Ion Batteries from First-Principles Calculations. *J. Phys. Chem. C* **2014**, 118, 24274−24281.

(15) Berdiyorov, G. R. Effect of Surface Functionalization on the Electronic Transport Properties of $Ti_3C_2$ MXene. *EPL* **2015**, 111, 67002.

(16) Khazaei, M.; Arai, M.; Sasaki, T.; Chung, C.-Y.; Venkataramanan, N. S.; Estili, M.; Sakka, Y.; Kawazoe, Y. Novel Electronic and Magnetic Properties of Two-Dimensional Transition Metal Carbides and Nitrides. *Adv. Funct. Mater.* **2013**, 23, 2185−2192.

(17) Zhao, H.; Zhang, C.; Li, S.; Ji, W.; Wang, P. First-Principles Design of Silicene/$Sc_2CF_2$ Heterojunction as a Promising Candidate for Field Effect Transistor. *J. Appl. Phys.* **2015**, 117, 085306.

(18) Lee, Y.; Hwang, Y.; Chung, Y.-C. Achieving Type I, II, and III Heterojunctions Using Functionalized MXene. *ACS Appl. Mater. Interfaces* **2015**, 7, 7163−7169.

(19) Li, X.; Dai, Y.; Ma, Y.; Liu, Q.; Huang, B. Intriguing Electronic Properties of Two-Dimensional $MoS_2$/$TM_2$ $CO_2$(TM = Ti, Zr, or Hf) Hetero-Bilayers: type-II Semiconductors with Tunable Band Gaps. *Nanotechnology* **2015**, 26, 135703.

(20) Gan, L.-Y.; Zhao, Y.-J.; Huang, D.; Schwingenschlögl, U. First-Principles Analysis of $MoS_2$/$Ti_2C$ and $MoS_2$/$Ti_2CY_2$ (Y = F and OH) All-2D Semiconductor/Metal Contacts. *Phys. Rev. B: Condens. Matter Mater. Phys.* **2013**, 87, 245307.

(21) Li, L. Effects of the Interlayer Interaction and Electric Field on the Band Gap of Polar Bilayers: A Case Study of $Sc_2CO_2$. *J. Phys. Chem. C* **2016**, 120, 24857−24865.

(22) Khazaei, M.; Arai, M.; Sasaki, T.; Estili, M.; Sakka, Y. Two-dimensional Molybdenum Carbides: Potential Thermoelectric Materials of the MXene Family. *Phys. Chem. Chem. Phys.* **2014**, 16, 7841−7849.

(23) Hu, Q.; Sun, D.; Wu, Q.; Wang, H.; Wang, L.; Liu, B.; Zhou, A.; He, J. MXene: A New Family of Promising Hydrogen Storage Medium. *J. Phys. Chem. A* **2013**, *117*, 14253−14260.

(24) Hu, Q.; Wang, H.; Wu, Q.; Ye, X.; Zhou, A.; Sun, D.; Wang, L.; Liu, B.; He, J. Two-dimensional Sc$_2$C: A Reversible and High-Capacity Hydrogen Storage Material Predicted by First-Principles Calculations. *Int. J. Hydrogen Energy* **2014**, *39*, 10606−10612.

(25) Yu, X.-F.; Li, Y.-C.; Cheng, J.-B.; Liu, Z.-B.; Li, Q.-Z.; Li, W.-Z.; Yang, X.; Xiao, B. Monolayer Ti$_2$CO$_2$: A Promising Candidate for NH$_3$ Sensor or Capturer with High Sensitivity and Selectivity. *ACS Appl. Mater. Interfaces* **2015**, *7*, 13707−13713.

(26) Mashtalir, O.; Cook, K.; Mochalin, V.; Crowe, M.; Barsoum, M.; Gogotsi, Y. Dye Adsorption and Decomposition on Two-Dimensional Titanium Carbide in Aqueous Media. *J. Mater. Chem. A* **2014**, *2*, 14334−14338.

(27) Lashgari, H.; Abolhassani, M.; Boochani, A.; Elahi, S.; Khodadadi, J. Electronic and Optical Properties of 2D Graphene-Like Compounds Titanium Carbides and Nitrides: DFT Calculations. *Solid State Commun.* **2014**, *195*, 61−69.

(28) Zha, X.-H.; Luo, K.; Li, Q.; Huang, Q.; He, J.; Wen, X.; Du, S. Role of the Surface Effect on the Structural, Electronic and Mechanical Properties of the Carbide MXenes. *EPL* **2015**, *111*, 26007.

(29) Zhang, X.; Ma, Z.; Zhao, X.; Tang, Q.; Zhou, Z. Computational Studies on Structural and Electronic properties of Functionalized MXene Monolayers and Nanotubes. *J. Mater. Chem. A* **2015**, *3*, 4960−4966.

(30) Yang, J.; Luo, X.; Zhang, S.; Chen, L. Investigation of Magnetic and Electronic properties of Transition Metal Doped Sc$_2$CT$_2$ (T = O, OH or F) Using a First Principles Study. *Phys. Chem. Chem. Phys.* **2016**, *18*, 12914−12919.

(31) Blöchl, P. E. Projector Augmented-Wave Method. *Phys. Rev. B: Condens. Matter Mater. Phys.* **1994**, *50*, 17953−17979.

(32) Kresse, G.; Joubert, D. From Ultrasoft Pseudopotentials to the Projector Augmented-Wave Method. *Phys. Rev. B: Condens. Matter Mater. Phys.* **1999**, *59*, 1758−1775.

(33) Kresse, G.; Furthmüller, J. Efficiency of Ab-Initio Total Energy Calculations for Metals and Semiconductors Using a Plane-Wave Basis Set. *Comput. Mater. Sci.* **1996**, *6*, 15−50.

(34) Perdew, J. P.; Burke, K.; Ernzerhof, M. Generalized Gradient Approximation Made Simple [Phys. Rev. Lett. 77, 3865 (1996)]. *Phys. Rev. Lett.* **1997**, *78*, 1396−1396.

(35) Monkhorst, H. J.; Pack, J. D. Special Points for Brillouin-Zone Integrations. *Phys. Rev. B* **1976**, *13*, 5188−5192.

(36) Togo, A.; Tanaka, I. First Principles Phonon Calculations in Materials Science. *Scr. Mater.* **2015**, *108*, 1−5.

(37) Kumar, S.; Schwingenschlögl, U. Thermoelectric Performance of Functionalized Sc$_2$C MXenes. *Phys. Rev. B: Condens. Matter Mater. Phys.* **2016**, *94*, 035405.